Nanoscale

Accepted Manuscript

Volume 8 | Number 1 | 7 January 2016 | Pages 1–660

Nanoscale

www.rsc.org/nanoscale

ISSN 2040-3364

ROYAL SOCIETY OF CHEMISTRY

PAPER
Qian Wang et al.
Ti₃C₂: a new two-dimensional sheet beyond MXenes

NCNST

This is an Accepted Manuscript, which has been through the Royal Society of Chemistry peer review process and has been accepted for publication.

Accepted Manuscripts are published online shortly after acceptance, before technical editing, formatting and proof reading. Using this free service, authors can make their results available to the community, in citable form, before we publish the edited article. We will replace this Accepted Manuscript with the edited and formatted Advance Article as soon as it is available.

You can find more information about Accepted Manuscripts in the author guidelines.

Please note that technical editing may introduce minor changes to the text and/or graphics, which may alter content. The journal's standard Terms & Conditions and the ethical guidelines, outlined in our author and reviewer resource centre, still apply. In no event shall the Royal Society of Chemistry be held responsible for any errors or omissions in this Accepted Manuscript or any consequences arising from the use of any information it contains.

Pseudocapacitive Behavior of Fe_2O_3 Anode and Its Contribution to High Reversible Capacity in Lithium Ion Batteries

Yimo Xiang,[a] Zhigao Yang,[a] Shengping Wang,[a]* Md. Shahriar A. Hossain,[b,c]
Jingxian Yu,[d] Nanjundan Ashok Kumar[c]* and Yusuke Yamauchi[b,c,e,f]*

a   Faculty of Materials Science and Chemistry, China University of Geosciences, Wuhan 430074, China

b   College of Chemistry and Molecular Engineering, Qingdao University of Science and Technology, Qingdao 266042, China

c   School of Chemical Engineering, School of Mechanical & Mining Engineering, and Australian Institute for Bioengineering and Nanotechnology (AIBN), The University of Queensland, Brisbane, QLD 4072, Australia

d   ARC Centre of Excellence for Nanoscale BioPhotonics (CNBP) and School of Chemistry and Physics, The University of Adelaide, Adelaide, SA 5005, Australia

e   Department of Plant & Environmental New Resources, Kyung Hee University, 1732 Deogyeong-daero, Giheung-gu, Yongin-si, Gyeonggi-do 446-701, South Korea

f   International Center for Materials Nanoarchitectonics (WPI-MANA), National Institute for Materials Science (NIMS), 1-1 Namiki, Tsukuba, Ibaraki 305-0044, Japan

   * E-mail: spwang@cug.edu.cn (S. Wang)
   * E-mail: ashok.kumar@uq.edu.au (N. A. Kumar)
   * E-mail: y.yamauchi@uq.edu.au (Y. Yamauchi)

Abstract:

Pseudocapacitance, which stores charge based on continuous and fast reversible redox reactions at the surface of electrode materials, is commonly observed in electrodes for lithium ion batteries, especially for transition metal oxide anodes. In this report, bare Fe_2O_3 of granular morphology (~30 nm in diameter) with high purity and decent crystallinity as well as recommendable electrochemical performances is fabricated hydrothermally and employed as the subject to clarify pseudocapacitive behavior in transition metal oxide anodes. Electrochemical technologies such as galvanostatic charging/discharging, differential capacity analysis (dQ/dV) and the power law relationship ($i=av^b$), which can distinguish pseudocapacitive behaviors of an electrode reaction were employed to analyze the electrodes. Reversible capacities of ~120 mAh g^{-1} (0.117 F cm^{-2}) for Fe_2O_3 were found within particular electrochemical windows (2.3~3.0 V, 0.3~0.8 V for discharging and 2.2~3.0 V, 0.3~1.3 V for charging). A new direction of optimizing the capacities, rate and cycling performances for lithium ion batteries is pointed out with connections between the pseudocapacitive behavior and morphologies of surfaces as well as structures of the electrodes.

Key words: Pseudocapacitance; Fe_2O_3; Lithium ion batteries.

2

1. Introduction

Transition metal oxides MO (M=Co, Ni, Cu, Fe and so forth) as anodes for lithium ion batteries was reported by P. Poizot and co-workers in 2000.[1] Reactions between MO and Li^+ are quite different from the (de)intercalation of Li^+ into the crystal of $Li_4Ti_5O_{12}$[2] and Li-alloy process in SnO.[3] The final products of MO and Li^+ are metallic nanoparticles (M) in the range of 1~5 nm and Li_2O[1]. Subsequently, for the reason of high theoretical capacity density, more kinds of transition metal oxides were evaluated, including Fe_2O_3,[4] Co_3O_4,[5] TiO_2,[6] Fe_3O_4,[7] CuO,[8] NiO[9] and so forth.

Ample number of reports focus on the efforts to relieve the volume changes during the electrode reactions,[10, 11] which results in poor electrochemical performances. With porous and void structures such as nanotube,[12, 13] nanowire array,[14] hollow sphere,[15] peapod-like structure,[16] porous particles,[4, 17] three-dimensional hollow structure[18-20] and so on, the cycling and rate performances were optimized efficiently.[4, 12-26] However, special electrochemical phenomena of transition metal oxides were also observed in the reports, e.g., V_2O_5,[27] Co_3O_4,[28] Fe_2O_3,[29] RuO_2.[30] Namely, high reversible capacities exceeding the theoretical values were obtained. For example, Fe_2O_3 delivered overflowing capacities (1007 mAh g^{-1} for theoretical capacity density[31]) for tens even hundreds of cycles, as listed in Table 1.

Table 1 Brief summarizations of the unusual electrochemical behavior for Fe_2O_3 (N in Table 1 represents the number of cycles in which the charging and discharging capacities exceed the theoretical value. It is worth noticing that N is limited by the data provided in the corresponding reference. For example, in a certain report, capacities of 150 cycles overflow the theoretical value, but only data of 100 cycles are provided. Under this circumstance, N here equals to 100)

transition metal oxide	1st discharge capacity (mAh g^{-1})	Current density (mA g^{-1})	Electrochemical window (V vs. Li^+/Li)	N	Ref.
	1233	100	0.01-3.0	100	[32]
	1494	100	0.005-3.0	10	[33]
Fe_2O_3	1251	100	0.05-3.0	100	[34]
	1330	300	0.01-3.0	190	[35]
	1705	200	0-3.0	100	[29]

Such capacities are quite unique and worth discussing for at least 3 reasons, 1) high reversibility, 2) capacities exceeding the theoretical value, and 3) existing for quite a number of cycles. Unambiguous reasons and detailed characteristics for this part of capacities are not only essential for the understanding of multiple Li^+ storage mechanisms in transition metal oxides, but also essential for the controllable application potential of such capacities to optimize the capacities and cycling performances of transition metal oxides.

During the initial several cycles, discharge and charge capacities in excess of 1007 mAh g^{-1} may be explained with the formation[36-38] and partial dissolution[36] of solid electrolyte interface (SEI), respectively. However, SEI turns to be stable and barely contributes to capacities after approximately 5 cycles.[37, 38] Thus, SEI was most commonly ascribed to clarify the "irreversible charge loss" (ICL) in the first cycle,[37, 39] instead of properly explaining highly reversible capacities exceeding the theoretical value for tens or hundreds of cycles. Therefore, sources of such reversible capacities are left to be explored from other aspects.

Pseudocapacitance, which is one kind of electrochemical procedures different from the faradic process controlled by solid phase diffusion, stores charge based on continuous and fast reversible redox reactions at the surface of electrode materials, especially for transition metal oxide anodes.[40, 41] Pseudocapacitive contribution in transition metal oxides was not only demonstrated with differential capacity (dQ/dV) curves,[42] but also proved to become increasingly important,[40, 41, 43-46] which resulted in reversible capacities exceeding the theoretical value for transition metal oxides including Fe_2O_3,[29, 32-35] Co_3O_4,[28, 47-49] RuO_2[30] and so forth. However, properties such as the amount and the electrochemical windows (a potential range within which pseudocapacitive capacities are delivered) of capacities resulted from pseudocapacitive behavior are still not clear enough. Specific amount and electrochemical windows benefit to the understanding of sources for overflowing capacities. More importantly, if the connections between the pseudocapacitive behavior and properties of its functional regions, which refer to the morphologies of the surfaces and structures of the electrodes, were built, controllable usage of pseudocapacitive capacities during the electrochemical processes of transition metal oxide anodes in lithium ion batteries, as well as the promotions of capacities, rate and cycling performances of lithium ion batteries would be realized. Thus, the exploration of pseudocapacitances in lithium ion batteries is an underdeveloped direction which is

so essential and promising for the future of lithium ion batteries that far more efforts should be paid on.

In this paper, hydrothermally synthesized Fe_2O_3 was employed to explore the characteristics of pseudocapacitive behavior for transition metal oxides. Galvanostatic charging/discharging and (dQ/dV) curves were used to provide the amount of pseudocapacitive capacities. The electrochemical windows of pseudocapacitive behavior were determined with power law relationship ($i=av^b$) between the currents at certain potentials of CV results and the scan rates. In this way, detailed features of capacities resulted from pseudocapacitive behavior in Fe_2O_3 were clarified, promoting the discovery of functional mechanism of pseudocapacitive behavior in Fe_2O_3, hence, making the controllable usage of such pseudocapacitance one step further. In addition, systematic electrochemical technologies developed and properties of pseudocapacitive behavior discovered can both be employed to the exploration of pseudocapacitcances for other transition metal oxides.

2. Experimental

2.1 Fabrication of Fe_2O_3

9 g glucose was dissolved into 65 mL deionized water with continuous stirring before transferring to a 100 mL sealed Teflon-lined autoclave for a hydrothermal process for 5 h at 190 ^{o}C. After vacuum filtration, washing with deionized water and ethanol for several times, drying at 65 ^{o}C for 12 h in an oven, brown powder was obtained. 36.3 g $Fe(NO_3)_3$ was dissolved into a mixed solvent formed with 20 mL deionized water and 10 mL ethanol. Then, 0.6 g brown powder was ultrasonically dispersed into the solution. After a reaction at 30 ^{o}C for 6 h in water bath with continuous stirring, the precursor was obtained with vacuum filtration and drying at 65 ^{o}C for 12 h. Finally, with a calcining process at 500 ^{o}C (with a heating rate of 2 ^{o}C min^{-1}) for 1 h in air, red Fe_2O_3 was obtained.

2.2 Electrochemical measurements

Test cells were fabricated utilizing Fe_2O_3 with acetylene black and polyvinylidene difluoride (PVDF) as the working electrode with the surface area of ~1.77 cm^2 (15 mm in diameter and 250 μm in thickness with ~1.45 mg Fe_2O_3). In detail, active material (60 wt.%), acetylene black (30 wt.%) and PVDF binder (10 wt.%) were dispersed in N-methy l-2-pyrrolidinone (NMP) solvent and stirred thoroughly to form

a slurry. The slurry was spread onto copper foil and maintained at 120 °C in an oven overnight. A metallic lithium plate was used as the counter electrode. Celgard 2400 was used as a separator. The electrolyte was 1 mol L^{-1} $LiPF_6$ in a 1:1 (volume ratio) mixture of ethylene carbonate (EC) and dimethyl carbonate (DMC).

Galvanostatic charging and discharging was evaluated with an Arbin BT2000 multichannel galvanostat in the potential range of 0.01~3.00 V (vs. Li/Li$^+$) at a current density of 0.1 and 10 mA cm^{-2}, respectively. Cyclic voltammetry (CV) tests were conducted on a VMP3 (Biologic) electrochemical workstation at various scan rate within 0.01~3.00 V (vs. Li$^+$/Li). Electrochemical impedance spectroscopy (EIS) were also conducted on a VMP3 (Biologic) electrochemical workstation with a frequency range of 10^5~10^{-2} Hz using a sine wave of 5 mV in the charging state (3 V vs. Li$^+$/Li) of the testing batteries employing Fe_2O_3 as active materials.

2.3. Characterizations

The phase structure of the product was determined by powder X-ray diffraction (XRD) on a Bruker AXS D8-FOCUS diffractometer with Cu Kα radiation. The morphology was observed by transmission electron microscopy (TEM, Philips CM12).

3. Results and discussion

3.1 Phase and morphology characterizations

As shown in Fig. 1, hydrothermally fabricated Fe_2O_3 can be indexed to rhombohedral iron oxide with JCPDS card number of 33-0664 (a=b=5.036 Å, c=13.749 Å, α=β=90º, γ=120º), indicating decent crystallinity and purity of Fe_2O_3.
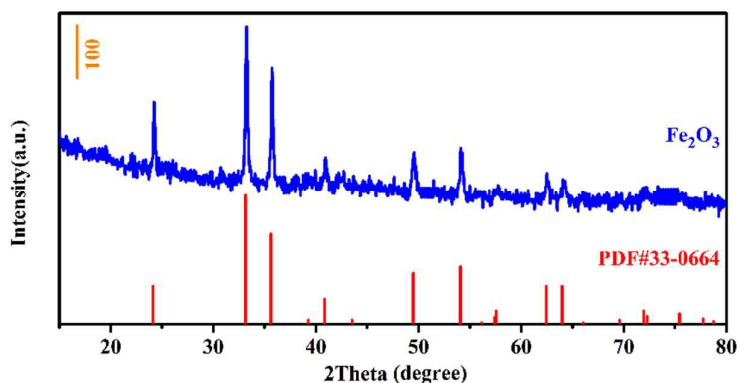

Figure 1. XRD pattern of Fe_2O_3.

TEM pictures in Fig. 2 display the morphology of Fe_2O_3. Instead of agglomerating, particles with diameter about 30 nm form three-dimensional interconnected structure. As shown in Fig. 2a, porous and void structures are observed. Single particle is display in Fig. 2b (inset).
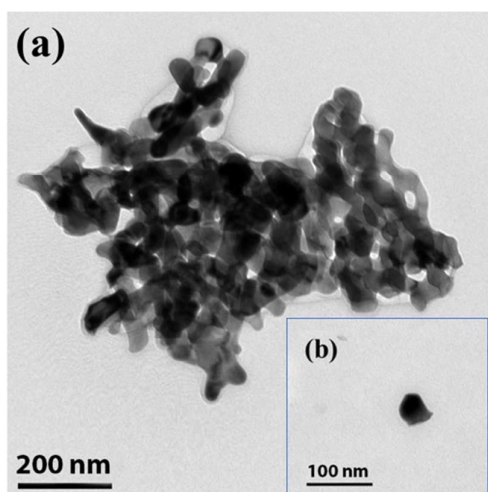

Figure 2. TEM images of Fe_2O_3.

3.2 Basic electrochemical measurements

Fig. 3 shows the CV results of Fe_2O_3. A reduction peak at ~0.39 V and an oxidation peak at ~1.79 V for the 1st cycle is noticed. In the following cycles, the reduction peak shifts to ~0.84 V while oxidation peak moves to ~1.90 V before the peak potentials and peak currents stabilizing. This couple of redox peaks corresponds to transformation reactions between Fe_2O_3 and Fe.[50, 51]
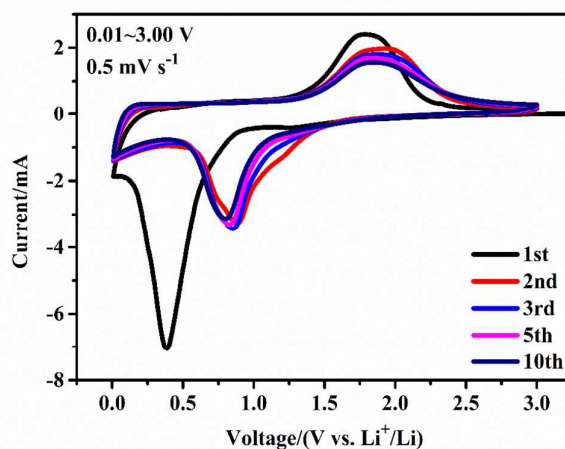

Figure 3. CV results of Fe_2O_3 at 0.5 mV s^{-1} within 0.01~3.00 V.

Charging and discharging curves of Fe_2O_3 at 0.1 mA cm^{-2} for the 1st, 2nd, 3rd, 5th and 10th cycles are shown in Fig. 4. There are two plateaus in the 1st discharging curve. The one at ~1.0 V corresponds to the reduction of Fe_2O_3 to Fe.[50, 52, 53] The formation of solid electrolyte interface (SEI) generates the other one at ~0.85 V[50, 54] and the 1st discharging capacity as high as 2308.7 mAh g^{-1}, which is far more than the theoretical value of 1007 mAh g^{-1}.[55] The plateau at ~1.75 V in the 1st charging curve corresponds to the transformation from Fe to Fe_2O_3. The charging capacity of the 1st cycle is 1157.24 mAh g^{-1}, which is also slightly higher than the theoretical value. During the following cycles, the plateau at ~0.85 V disappears from the discharging curves while the plateaus in the charging curves barely change. Capacities decay slowly with the increasing cycle number. The discharging and charging capacity of the 10th cycle is 1042.95 and 1007.09 mAh g^{-1}, respectively, still higher than the theoretical value.
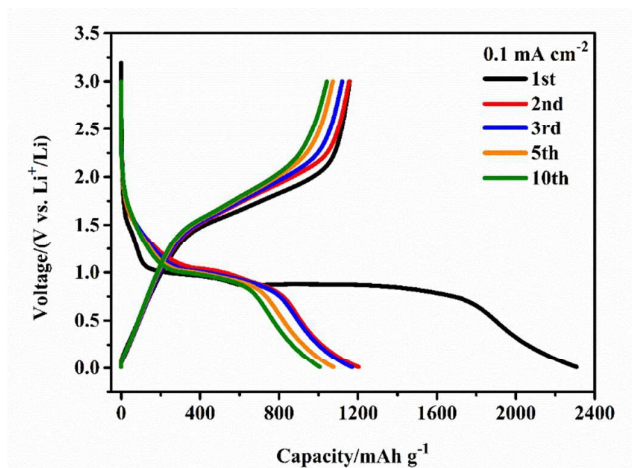
Figure 4. Charging and discharging curves of Fe_2O_3 at 0.1 mA cm^{-2} within 0.01~3.00 V.

3.3 Preliminary analysis of pseudocapacitive behavior in Fe_2O_3

As demonstrated with XRD, TEM and basic electrochemical tests including CV and galvanostatic charging and discharging, the prepared Fe_2O_3 is proved to exhibit good quality and stable electrochemical performances for the exploration of pseudocapacitive behavior. Fig. 5 indicates the cycling performances of Fe_2O_3 at 0.1 mA cm^{-2} during the initial 100 cycles. In Fig. 5a, capacities and the corresponding Coulombic efficiency for 100 cycles are displayed. With Coulombic efficiency of nearly 100%, capacities maintain around 1000 mAh g^{-1} after 5 cycles for the stabilization of SEI. Apart from the initial 10 cycles (highlighted in Fig. 5b), capacities vary obviously within 40th~66th cycles, showing a tendency of increasing first and then decreasing, as shown in Fig. 5c. More importantly, the capacities within 1st~10th and 40th~66th cycles overflow the theoretical value of 1007 mAh g^{-1}. As mentioned in the introduction, capacities for the first 5 cycles can be influenced by SEI. For this case, if the reversible capacities observed in the initial 10 cycles were caused by SEI. Then, the same phenomenon occurred during 40th~66th cycles cannot be explained with SEI precisely. Thus, pseudocapacitive behavior of Fe_2O_3 should be taken into consideration and explored carefully.
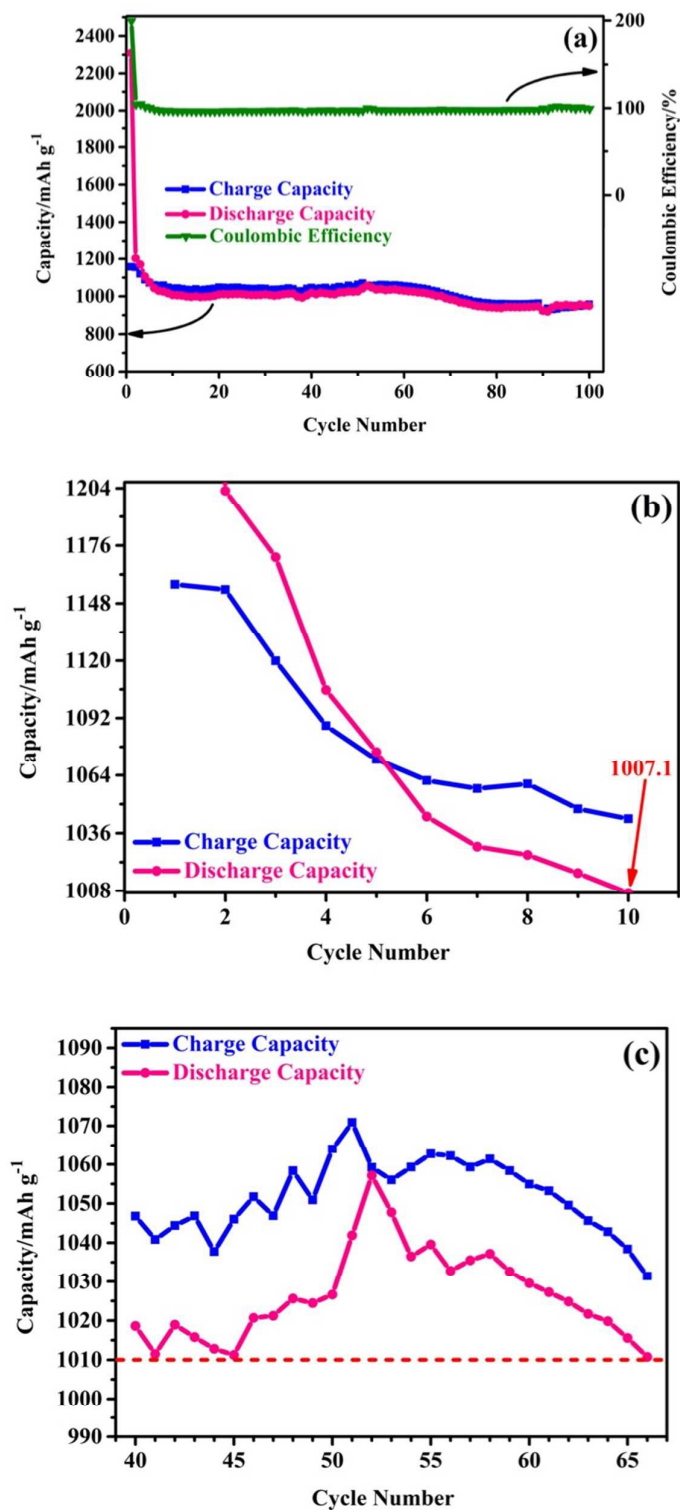
Figure 5. Capacities of Fe_2O_3 at 0.1 mA cm^{-2} for (a) the initial 100 cycles, (b) the initial 10 cycles, and (c) 40th~66th cycles.

3.4 Pseudocapacitive capacity measured with galvanostatic charging and discharging

Stable and highly reversible capacities under high rates of transition metal oxides reflect their pseudocapacitive behavior,[45, 56] stable and reversible capacities under 4C of RuO_2 for example.[45, 57] Thus, galvanostatic charging and discharging at high current densities can be employed as one of the electrochemical techniques to clarify pseudocapacitive behavior.

Aiming at avoiding the effects of SEI, the testing battery was processed with low current density of 0.1 mA cm^{-2} for 5 cycles. The results revealed in Fig. 6a provides the same information reflected in Fig. 4. Namely, before the capacities stabilizing at ~1100 mAh g^{-1} in the 5th cycle, 2 discharging plateaus and large ICL are observed in the 1st cycle. In the following galvanostatic process, current density of 10 mA cm^{-2} (approximately 12.2 A g^{-1}, 12C) was applied to the test. Fig. 6b shows the charging and discharging curves for the 100th cycle at 10 mA cm^{-2}, which is quite close to the shapes of charging and discharging curves for capacitors.[42, 58] Highly reversible (Coulombic efficiency of 100%) capacities as high as ~120 mAh g^{-1} are also observed in Fig. 6c under 10 mA cm^{-2} for 100 cycles (excluding the initial 5 cycles under 0.1 mA cm^{-2}), confirming the existence of pseudocapacitive capacities in Fe_2O_3. Capacity here is converted into pseudocapacitance with Eq. 1, in which Q is the capacity (mAh g^{-1}), g is the mass of active materials (0.00145 g), U is the voltage (2.99 V), S is the area of the electrode (1.77 cm^2), 3.6 is used to transfer mAh to C. As displayed in Fig. 6c, pseudocapacitance over 0.117 F cm^{-2} is obtained for 100 cycles.

$$C=3.6\frac{Q{\cdot}g}{U{\cdot}S} \quad (1)$$

It is worth noticing that, same tendency in Fig. 5a is exhibited in Fig. 6c. Namely, capacities increase slowly from the 20th cycle, approaching the maximum value at ~50th cycle before decreasing to the original value at ~80th cycle. Such variation is caused by the unique products in the reduction of Fe_2O_3. Metallic Fe nanoparticles with high conductivity and electrochemical inactive Li_2O are generated after discharging the testing batteries. During the following charging process, state of Fe and Li_2O will change gradually until the majority of Fe and Li_2O convert to Fe_2O_3 at the end of the oxidation reaction. Thus, during the cycles, interface of Fe and Li_2O, as

well as the conditions and electrochemical activities of the particle surface will change slightly as reactions progressing, influencing the reactions occurred on the surface, which is exactly the pseudocapacitive reaction.[45, 59] Therefore, the same tendency shown in Fig. 5a and 6c is brought about by pseudocapacitance. In conclusion, pseudocapacitive capacity over 120 mAh g^{-1} (pseudocapacitance over 0.117 F cm^{-2}) is determined with galvanostatic charging and discharging at high rate, which possesses high reversibility during 100 cycles and constitutes ~10% of the whole amount of reversible capacity.

3.5 Pseudocapacitive capacity measured with differential capacity (dQ/dV) curves

The combination of (dis)charging profiles and dQ/dV curves was proved to be able to distinguish pseudocapacitive behavior from other processes in a battery system.[42, 58, 60, 61] Fig. 7a and b display the 6th discharging curve as well as its corresponding dQ/dV curve and 6th charging curve as well as its corresponding dQ/dV curve at 0.1 mA cm^{-2}, respectively. In the 6th discharging process (Fig. 7a), there is a peak within 0.58~1.57 V, which corresponding to the faradic process controlled by solid phase diffusion. A small amount of contribution from SEI still exists below 0.19 V.[42]

Other than these regions, capacity of 54.52 mAh g^{-1} above 1.57 V and 156.02 mAh g^{-1} in 0.19~0.58 V, can be attributed to the pseudocapacitances. Namely, pseudocapacitive capacity separated with dQ/dV curve for the 6th cycle at 0.1 mA cm^{-2} is 210.54 mAh g^{-1} in total, which is quite close to the pseudocapacitive capacity of 217.76 mAh g^{-1} (1st cycle in Fig. 6c) measured with galvanostatic charging and discharging at high rate. Fig. 7c shows the pseudocapacitive capacities determined with dQ/dV curves from the galvanostatic charging and discharging results at 0.1 mA cm^{-2} between 6th cycle and 105th cycle. Within the 100 cycles displayed, pseudocapacitive capacities of more than 120 mAh g^{-1} as well as a tendency of increasing slowly from the 20th cycle, approaching the maximum value at ~60th cycle before decreasing to the original value at ~80th cycle for the capacities, are observed. Both of the phenomenon closely approximates the behavior revealed in Fig. 6c. Thus, during the 100 cycles discussed for Fe$_2$O$_3$, combination of (dis)charging profiles and dQ/dV curves proved the existence of pseudocapacitive capacities of ~120 mAh g^{-1}.
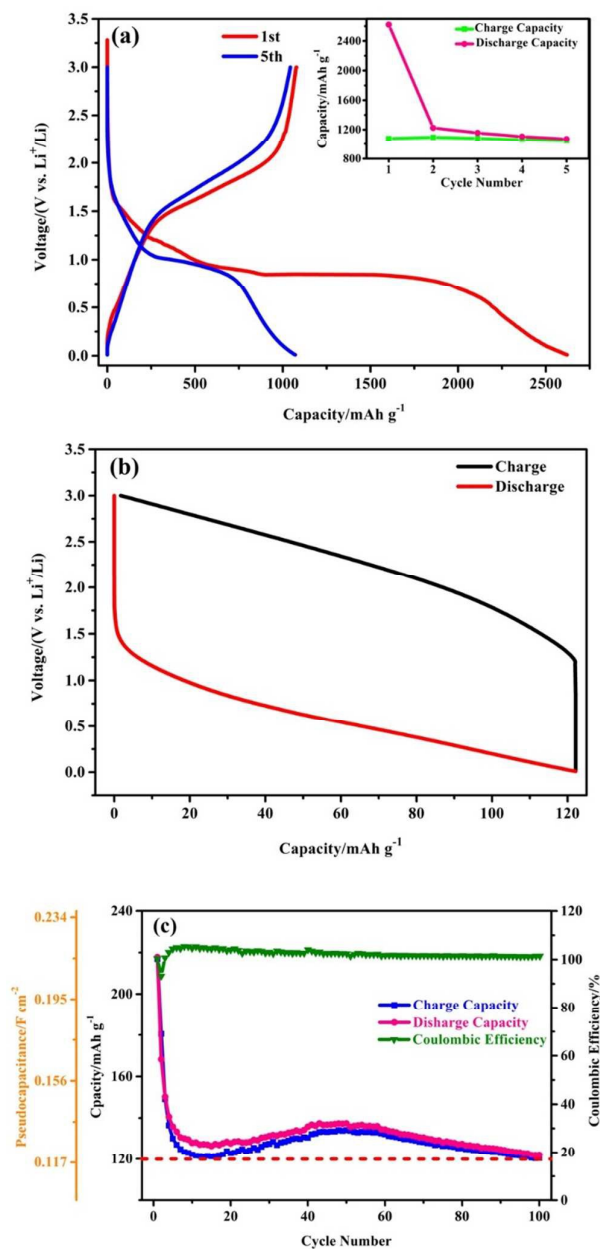
Figure 6. Charging and discharging curves of (a) the 1st and 5th cycles at 0.1 mA cm^{-2}, (b) the 100th cycles at 10 mA cm^{-2}, and (c) capacities and Coulombic efficiency for the first 100 cycles (excluding the initial 5 cycles at 0.1 mA cm^{-2}) at 10 mA cm^{-2}.
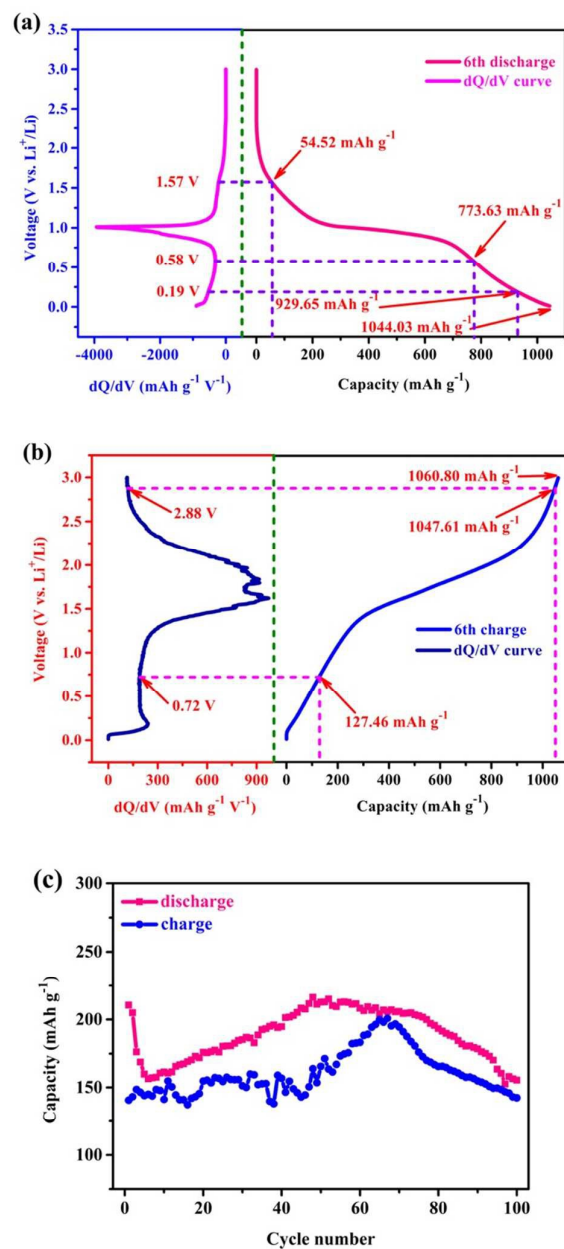
Figure 7. (a) The discharging curve and its differential capacity curve of the 6th cycle at 0.1 mA cm^{-2}, (b) The charging curve and its differential capacity curve of the 6th cycle at 0.1 mA cm^{-2}, (c) capacities contributed with pseudocapacitance at 0.1 mA cm^{-2} separated with differential capacity curves.

3.6 Pseudocapacitive electrochemical windows determined with $i=av^b$

In the linear sweep voltammetry for reversible systems with concentration polarization, the relationship between the current and potential can be expressed with Eq. 2, in which n is the number of electrons involved in the reaction, F is the faraday constant, A is the surface area of the electrode, D is the Li$^+$ diffusion coefficient, v is the scan rate, R is the gas constant, T is the temperature, $\pi^{0.5}\chi(\sigma t)$ is the dimensionless current function. The dimensionless current function is a dimensionless variable which possesses a definite correspondence with the current. It is defined to translate the relation between current and time into relation between current and potential with $\sigma t = (nF/RT) \cdot vt$.[62]

When $\pi^{0.5}\chi(\sigma t)$ approaching its extreme value 0.4463, Eq. 2 can be transformed into Eq. 3, in which C_0 is the initial concentration of the reactants, i_p is the peak current in the CV curve.

$$i = nFAC_0D^{0.5}v^{0.5}\left(\frac{nF}{RT}\right)^{0.5}\pi^{0.5}\chi(\sigma t) \tag{2}$$

$$i_P = (2.69 \times 10^5)n^{1.5}AD^{0.5}v^{0.5}C_0 \ (25°C) \tag{3}$$

Eq. 2 (at a certain potential) and Eq. 3 can be transformed into Eq. 4 with a as an adjustable parameter. Namely, at a certain potential in the faradic process controlled by solid phase diffusion, the measured current i obeys a power law relationship with the scan rate v as illustrated with Eq. 4. While the pure capacitive current is proportional to the sweep rate, according to Eq. 5,[63] in which C_d is the capacitance, $a = C_d A$.

$$i = av^{0.5} \tag{4}$$

$$i = vC_d A = av^1 \tag{5}$$

Thus, Eq. 6 is built to distinguish faradic process controlled by solid phase diffusion, pure capacitive process and pseudocapacitive process with a and b as adjustable parameters. With $b=0.5$, current caused with the faradic process controlled by solid phase diffusion is dominant. When $b=1$, capacitive current is the principal contribution. While at the case of ~0.8<b<1, the current is mainly aroused with the pseudocapacitances.[43, 63]

$$i = av^b \tag{6}$$

$$\log i = b\log v + \log a \tag{7}$$

With CV results under different scan rates, the value of b can be obtained with linear relationship between $\log i$ and $\log v$ after transforming Eq. 6 to Eq. 7, hence, whether the pseudocapacitance is the dominant source for the measured current can be determined with the b value. Furthermore, with a function $i(V)$ to express the measured current at a certain potential, as shown in Eq. 8, current from the faradic process controlled by solid phase diffusion ($k_2 v^{0.5}$) and capacitive current ($k_1 v$) can be separated. And Eq. 9, which is another expression of Eq. 8, can be employed to determine the parameters k_1 and k_2.

$$i(V) = k_1 v + k_2 v^{0.5} \tag{8}$$

$$\frac{i(V)}{v^{0.5}} = k_1 v^{0.5} + k_2 \tag{9}$$

The value of b obtained with Eq. 7 and capacitive current ($k_1 v$) separated with Eq. 8, both can clarify the features of pseudocapacitances. Thus, CV tests under scan rate of 0.1, 0.2, 0.3, 0.4, 0.5, 0.6, 0.7, 0.8, 0.9 and 1.0 mV s^{-1} were conducted on the batteries with Fe_2O_3 as the active material. As shown in Fig. 8a, there is a pair of apparent redox peaks in each of the curves obtained. Peak currents and differences between reduction and oxidation peaks both increase with the rise of scan rates.

The values of b, together with the parameters of k_1 and k_2, at the potential of 0.01 V and 3.0-0.1n V ($0 \leq n \leq 29$) are obtained with results shown in Fig. 8a. The variation tendency of b values is shown in Fig. 8b. Proportions of capacitive current ($k_1 v$) increase with the scan rates, are shaded in gray as shown in Fig. 8c (0.3 mV s^{-1}), Fig. 8d (0.5 mV s^{-1}), Fig. 8e (0.8 mV s^{-1}) and Fig. 8f (1 mV s^{-1}). Conversion of electrode processes shown in Fig. 8b and Fig. 8c-f are quite close to each other. That is, during the reduction reactions, in the range of about 0.01~0.2 V and 0.9~2.2 V, the electrode reactions are dominated by faradic process controlled by solid phase diffusion. Pseudocapacitive behavior mainly take place within 2.3~3.0 V and 0.3~0.8 V. While during the oxidation reactions, in the range of about 0.01~0.2 V and 1.4~2.1 V, the electrode reactions are dominated by faradic process controlled by solid phase diffusion. Pseudocapacitive behavior mainly take place within 2.2~3.0 V and 0.3~1.3 V. In conclusion, the main pseudocapacitive electrochemical windows determined with $i=av^b$ are 2.3~3.0 V and 0.3~0.8 V for the reduction reactions, 2.2~3.0 V and 0.3~1.3 V for oxidation reactions.
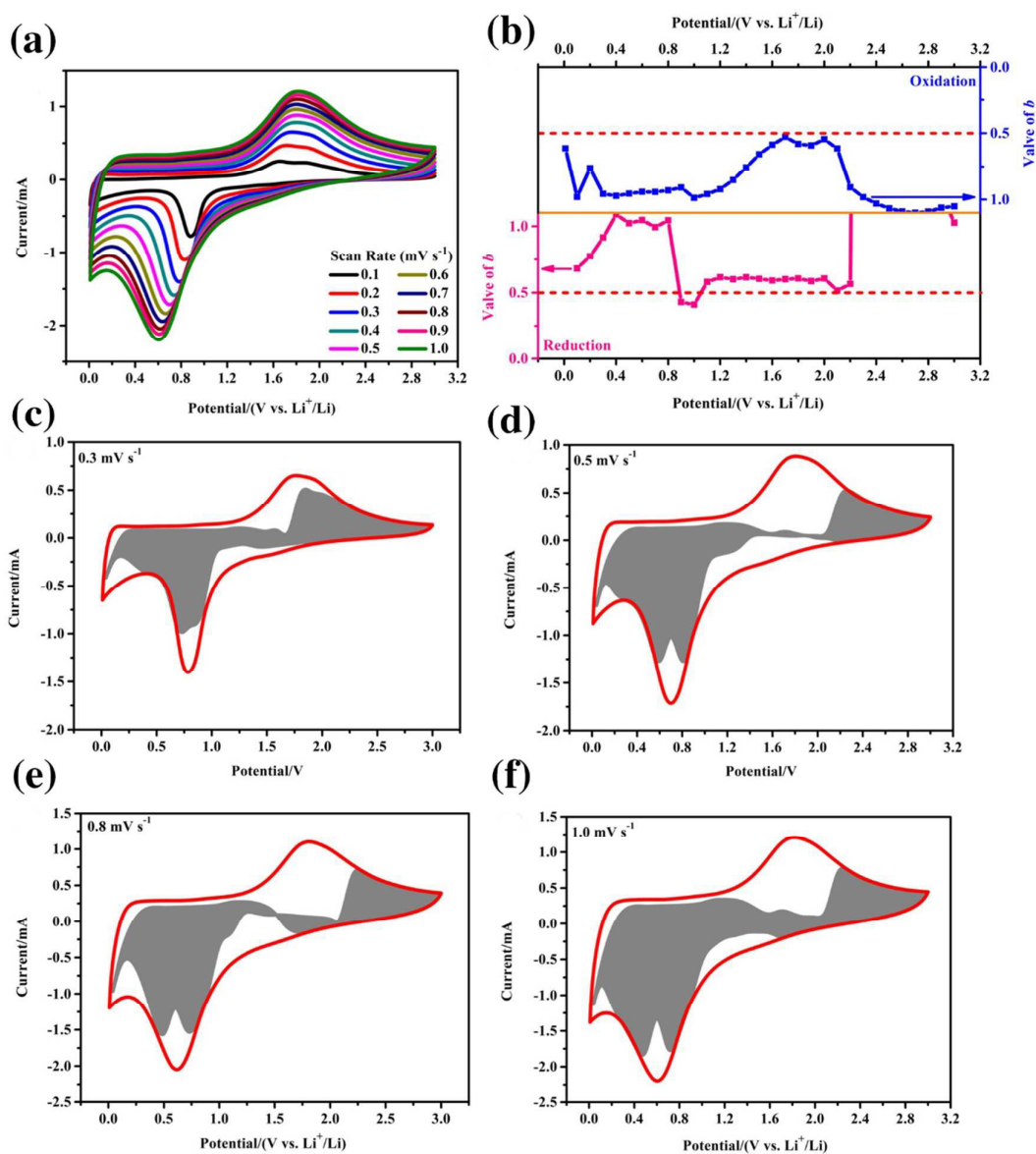
Figure 8. (a) CV results at 0.1, 0.2, 0.3, 0.4, 0.5, 0.6, 0.7, 0.8, 0.9 and 1.0 mV s^{-1}, (b) Variation tendency of the values of *b*, the areas that the pseudocapacitance contributions take up in the CV curve at 0.3 mV s^{-1} (c), 0.5 mV s^{-1} (d), 0.8 mV s^{-1} (e) and 1 mV s^{-1} (f).

4. Conclusions

In the measurements of cycling performance of granular Fe_2O_3 (~30 nm of diameter) at 0.1 mA cm^{-2}, highly reversible capacities within 1st~10th and 40th~66th cycles overflowing the theoretical value were noticed. Pseudocapacitive contribution to the capacity was pointed out and proved after ruling out the influences of SEI. The detailed amount of pseudocapacitive capacities were separated from the total reversible capacities, and the electrochemical windows within which the pseudocapacitive behavior take place were reported here. These discoveries will shine a light on new approaches to modify the capacities of transition metal oxides.

1) With galvanostatic charging and discharging test at high rate (10 mA cm^{-2}), pseudocapacitive contributions of ~120 mAh g^{-1} for 100 cycles were obtained, which occupy ~10% of the total reversible capacities and corresponding to pseudocapacitances over 0.117 F cm^{-2}. dQ/dV curves of the galvanostatic charging and discharging results between 6th to 105th cycles at 0.1 mA cm^{-2} were used to separate the pseudocapacitive capacities, with which pseudocapacitive contributions over 120 mAh g^{-1} were also found.

2) Analysis based on the power low between the response current and scan rates ($i=av^b$) with CV results under various scan rates found out that, pseudocapacitive behavior mainly take place within 2.3~3.0 V, 0.3~0.8 V during the reduction reactions and within 2.2~3.0 V, 0.3~1.3 V for the oxidation reactions.

Intrinsic reason for the reversible capacities overflowing theoretical value delivered by Fe_2O_3 was clarified as pseudocapacitive behavior, which is obviously different from the explanation of SEI formation. More importantly, the amount of pseudocapacitive capacities and its electrochemical windows were quantized. High reversible capacities contributed with such pseudocapacitances, showing different features from capacities delivered by traditional batteries reactions, possess decent cycling performances. This uncommon discovery and specialized discussion of pseudocapacitive capacities pointed out a new direction of increasing the reversible capacities of transition metal oxides, that will exhibit huge application potentiality.

Acknowledgments

References:

1.   P. Poizot, S. Laruelle, S. Grugeon, L. Dupont and J. M. Tarascon, *Nature*, 2000, **407**, 496.

2.   Y.-Q. Wang, L. Gu, Y.-G. Guo, H. Li, X.-Q. He, S. Tsukimoto, Y. Ikuhara and L.-J. Wan, *J. Am. Chem. Soc.*, 2012, **134**, 7874-7879.

3.   H. Li, X. Huang and L. Chen, *J. Power Sources*, 1999, **81-82**, 335-339.

4.   X. Xu, R. Cao, S. Jeong and J. Cho, *Nano Letters*, 2012, **12**, 4988-4991.

5.   G. Huang, S. Xu, S. Lu, L. Li and H. Sun, *ACS Appl. Mater. & Int.*, 2014, **6**, 7236-7243.

6.   Y.-H. Ding, P. Zhang, H.-M. Ren, Q. Zhuo, Z.-M. Yang and Y. Jiang, *Mater. Res. Bull.*, 2011, **46**, 2403-2407.

7.   G. Zhou, D.-W. Wang, F. Li, L. Zhang, N. Li, Z.-S. Wu, L. Wen, G. Q. Lu and H.-M. Cheng, *Chem. Mater.*, 2010, **22**, 5306-5313.

8.   B. Wang, X.-L. Wu, C.-Y. Shu, Y.-G. Guo and C.-R. Wang, *J. Mater. Chem.*, 2010, **20**, 10661-10664.

9.   H. Liu, G. Wang, J. Liu, S. Qiao and H. Ahn, *J. Mater. Chem.*, 2011, **21**, 3046-3052.

10.   L. Ji, Z. Lin, M. Alcoutlabi and X. Zhang, *Energy & Environ. Sci.*, 2011, **4**, 2682-2699.

11.   P. Poizot, S. Laruelle, S. Grugeon and J.-M. Tarascon, *J. Electrochem. Soc.*, 2002, **149**, A1212-A1217.

12.   N. Du, H. Zhang, B. D. Chen, J. B. Wu, X. Y. Ma, Z. H. Liu, Y. Q. Zhang, D. R. Yang, X. H. Huang and J. P. Tu, *Adv. Mater.*, 2007, **19**, 4505-4509.

13.   J. Chen, L. Xu, W. Li and X. Gou, *Adv. Mater.*, 2005, **17**, 582-586.

14.   Y. Li, B. Tan and Y. Wu, *Nano Lett.*, 2008, **8**, 265-270.

15.   X. Rui, H. Tan, D. Sim, W. Liu, C. Xu, H. H. Hng, R. Yazami, T. M. Lim and Q. Yan, *J. Power Sources*, 2013, **222**, 97-102.

16.   Y. Wang, H. J. Zhang, L. Lu, L. P. Stubbs, C. C. Wong and J. Lin, *ACS Nano*, 2010, **4**, 4753-4761.

17.   J. S. Chen, T. Zhu, X. H. Yang, H. G. Yang and X. W. Lou, *J. Am. Chem. Soc.*, 2010, **132**, 13162-13164.

18.   B. Wang, J. S. Chen, H. B. Wu, Z. Wang and X. W. Lou, *J. Am. Chem. Soc.*, 2011, **133**, 17146-17148.

19.   Z. Wang, D. Luan, S. Madhavi, C. Ming Li and X. Wen Lou, *Chem. Commun.*,

2011, **47**, 8061-8063.

20.   L. Zhang, H. B. Wu, S. Madhavi, H. H. Hng and X. W. Lou, *J. Am. Chem. Soc.*, 2012, **134**, 17388-17391.

21.   X. Hu and J. C. Yu, *Adv. Funct. Mater.*, 2008, **18**, 880-887.

22.   Y. Han, Y. Wang, L. Li, Y. Wang, L. Jiao, H. Yuan and S. Liu, *Electrochimica Acta*, 2011, **56**, 3175-3181.

23.   D. Lei, M. Zhang, B. Qu, L. Chen, Y. Wang, E. Zhang, Z. Xu, Q. Li and T. Wang, *Nanoscale*, 2012, **4**, 3422-3426.

24.   M. V. Reddy, T. Yu, C. H. Sow, Z. X. Shen, C. T. Lim, G. V. Subba Rao and B. V. R. Chowdari, *Adv. Funct. Mater.*, 2007, **17**, 2792-2799.

25.   T. Yu, Y. Zhu, X. Xu, K.-S. Yeong, Z. Shen, P. Chen, C.-T. Lim, J. T.-L. Thong and C.-H. Sow, *Small*, 2006, **2**, 80-84.

26.   L. Zhang, H. B. Wu and X. W. Lou, *J. Am. Chem. Soc.*, 2013, **135**, 10664-10672.

27.   M. Sathiya, A. S. Prakash, K. Ramesha, J. M. Tarascon and A. K. Shukla, *J. Am. Chem. Soc.*, 2011, **133**, 16291-16299.

28.   X. Hou, J. He, K. An, J. Mu, X. Chou and C. Xue, *Appl. Surf. Sci.*, 2016, **383**, 159-164.

29.   X. Zhu, X. Jiang, X. Chen, X. Liu, L. Xiao and Y. Cao, *J. Alloys and Compounds*, 2017, **711**, 15-21.

30.   P. Balaya, H. Li, L. Kienle and J. Maier, *Adv. Funct. Mater.*, 2003, **13**, 621-625.

31.   J.-M. Jeong, B. G. Choi, S. C. Lee, K. G. Lee, S.-J. Chang, Y.-K. Han, Y. B. Lee, H. U. Lee, S. Kwon, G. Lee, C.-S. Lee and Y. S. Huh, *Adv. Mater.*, 2013, **25**, 6250-6255.

32.   Q. Li, H. Wang, J. Ma, X. Yang, R. Yuan and Y. Chai, *J. Alloys and Compounds*, 2018, **735**, 840-846.

33.   N. Shen, M. Keppeler, B. Stiaszny, H. Hain, F. Maglia and M. Srinivasan, *Beilstein J. Nanotechnol.*, 2017, **8**, 2032-2044.

34.   Y. Z. Wang, J. S. Han, X. X. Gu, S. Dimitrijev, Y. L. Hou and S. Q. Zhang, *J. Mater. Chem. A*, 2017, **5**, 18737-18743.

35.   Y. Zhao, X. Zhai, D. Yan, C. Ding, N. Wu, D. Su, Y. Zhao, H. Zhou, X. Zhao, J. Li and H. Jin, *Electrochimica Acta*, 2017, **243**, 18-25.

36.   P. Verma, P. Maire and P. Novák, *Electrochim. Acta*, 2010, **55**, 6332-6341.

37.   H. Bryngelsson, M. Stjerndahl, T. Gustafsson and K. Edström, *J. Power Sources*, 2007, **174**, 970-975.

38.   D. Alliata, R. Kötz, P. Novák and H. Siegenthaler, *Electrochem. Commun.*, 2000, **2**, 436-440.

39.   K. Zaghib, G. Nadeau and K. Kinoshita, *J. Electrochem. Soc.*, 2000, **147**, 2110-2115.

40.   S. Liu, S. Sun and X.-Z. You, *Nanoscale*, 2014, **6**, 2037-2045.

41.   J. Jiang, Y. Li, J. Liu, X. Huang, C. Yuan and X. W. Lou, *Adv. Mater.*, 2012, **24**, 5166-5180.

42.   F. Feng, S. Zhao, R. Liu, Z. Yang and Q. Shen, *Electrochimica Acta*, 2016, **222**, 1160-1168.

43.   J. Wang, J. Polleux, J. Lim and B. Dunn, *J. Phys. Chem. C*, 2007, **111**, 14925-14931.

44.   J. Jamnik and J. Maier, *Phys. Chem. Chem. Phys.*, 2003, **5**, 5215-5220.

45.   P. Balaya, A. J. Bhattacharyya, J. Jamnik, Y. F. Zhukovskii, E. A. Kotomin and J. Maier, *J. Power Sources*, 2006, **159**, 171-178.

46.   C. D. Lokhande, D. P. Dubal and O.-S. Joo, *Current Appl. Phys.*, 2011, **11**, 255-270.

47.   X. Yao, G. Guo, Y. Zhao, Y. Zhang, S. Y. Tan, Y. Zeng, R. Zou, Q. Yan and Y. Zhao, *Small*, 2016, **12**, 3849-3860.

48.   Y. Tan, Q. Gao, Z. Li, W. Tian, W. Qian, C. Yang and H. Zhang, *Sci. Rep.*, 2016, **6**, 26460.

49.   W. Gou, X. Zhou, J. Li and Y. Ma, *Mater. Lett.*, 2016, **180**, 207-211.

50.   S. Xu, C. M. Hessel, H. Ren, R. Yu, Q. Jin, M. Yang, H. Zhao and D. Wang, *Energy & Environ. Sci.*, 2014, **7**, 632-637.

51.   B. Sun, J. Horvat, H. S. Kim, W.-S. Kim, J. Ahn and G. Wang, *J. Phys. Chem. C*, 2010, **114**, 18753-18761.

52.   X. Pan, X. Duan, X. Lin, F. Zong, X. Tong, Q. Li and T. Wang, *J. Alloys and Compounds*, 2018, **732**, 270-279.

53.   M. Chen, J. Liu, D. Chao, J. Wang, J. Yin, J. Lin, H. Jin Fan and Z. Xiang Shen, *Nano Energy*, 2014, **9**, 364-372.

54.   J. Hu, C.-F. Sun, E. Gillette, Z. Gui, Y. Wang and S. B. Lee, *Nanoscale*, 2016, **8**, 12958-12969.

55.   F. Joho, B. Rykart, A. Blome, P. Novák, H. Wilhelm and M. E. Spahr, *J.

Power Sources, 2001, **97**, 78-82.

56.   S. Laruelle, S. Grugeon, P. Poizot, M. Dollé, L. Dupont and J.-M. Tarascon, *J. Electrochem. Soc.*, 2002, **149**, A627-A634.

57.   Y. F. Zhukovskii, P. Balaya, E. A. Kotomin and J. Maier, *Phys. Rev. Lett.*, 2006, **96**, 058302.

58.   A. G. Dylla, G. Henkelman and K. J. Stevenson, *Acc. Chem. Res.*, 2013, **46**, 1104-1112.

59.   Y. Kim, J.-H. Lee, S. Cho, Y. Kwon, I. In, J. Lee, N.-H. You, E. Reichmanis, H. Ko, K.-T. Lee, H.-K. Kwon, D.-H. Ko, H. Yang and B. Park, *ACS Nano*, 2014, **8**, 6701-6712.

60.   J. Y. Shin, D. Samuelis and J. Maier, *Adv. Funct. Mater.*, 2011, **21**, 3464-3472.

61.   S. Zhao, F. Feng, F. Yu and Q. Shen, *J. Mater. Chem. A*, 2015, **3**, 24095-24102.

62.   A. J. Bard, L. R. Faulkner, J. Leddy and C. G. Zoski, *Electrochemical methods: fundamentals and applications*, wiley New York, 1980.

63.   H. Lindström, S. Södergren, A. Solbrand, H. Rensmo, J. Hjelm, A. Hagfeldt and S.-E. Lindquist, *J. Phys. Chem. B*, 1997, **101**, 7717-7722.

Nanoscale Accepted Manuscript